Experimental and theoretical study of the transition between diffuse and contracted forms of the glow discharge in argon

2008 J. Phys. D: Appl. Phys. 41 055204

(http://iopscience.iop.org/0022-3727/41/5/055204)

IOP PUBLISHING JOURNAL OF PHYSICS D: APPLIED PHYSICS

J. Phys. D: Appl. Phys. **41** (2008) 055204 (14pp) doi:10.1088/0022-3727/41/5/055204

Experimental and theoretical study of the transition between diffuse and contracted forms of the glow discharge in argon

N A Dyatko[1], Y Z Ionikh[2], I V Kochetov[1], D L Marinov[2], A V Meshchanov[2], A P Napartovich[1], F B Petrov[2] and S A Starostin[3]

[1] State Research Center Troitsk Institute for Innovation and Fusion Research, 142190 Troitsk, Moscow Region, Russia
[2] Institute of Physics, St Petersburg University, 198904 St Petersburg, Russia
[3] Eindhoven University of Technology, Eindhoven, Netherlands

E-mail: dyatko@triniti.ru

Received 24 October 2007, in final form 7 January 2008
Published 14 February 2008
Online at stacks.iop.org/JPhysD/41/055204

Abstract

The constriction of the positive column of a glow discharge in argon was studied both experimentally and theoretically. In experiments the direct current discharge was maintained in a cylindrical glass tube of 3 cm internal diameter and 75 cm length. The voltage–current $U(I)$ characteristics of the discharge were measured at a gas pressure P from 1 to 120 Torr in a wide range of discharge currents. At $P > 20$ Torr the measured $U(I)$ characteristics display the classical hysteresis effect: the transition from the diffuse to the contracted discharge form (with increasing current) occurs at a current higher than that for reverse transition (with decreasing current). It was also found that in some cases the so-called partially contracted form of the discharge is realized, when the diffuse and contracted forms coexist in the discharge tube.

To calculate the plasma parameters under experimental conditions a 1D axial-symmetric discharge model for pure argon was developed. The details of the model are described and the results of simulations are presented. In particular, the electric field strength E in the positive column was calculated as a function of the discharge current. Theoretical $E(I)$ characteristics are compared with those derived from the experiment. For the first time, the detailed kinetic model without the usage of fit parameters predicts the hysteresis effect in pure Ar with parameters of diffuse and constricted forms of the discharge in good agreement with the experiment.

1. Introduction

It is well known that at intermediate gas pressures an increase in the discharge current leads to the constriction of the positive column of a diffuse glow discharge and the formation of a bright filament, the transverse size of which is small with respect to the discharge tube diameter [1–3]. The behaviour of the positive column during transition from the diffuse to the contracted form is diverse, dependent on the type of gas and pressure. In some cases this transition occurs gradually, i.e. the visible diameter of the plasma in the whole of the positive column diminishes gradually with the current increase. But in most cases another scenario is realized: stepwise transition to the contracted form as soon as the discharge current exceeds some critical value I_c.

During the last few decades the effect of discharge constriction in inert gases was comprehensively studied both experimentally [4–11] and theoretically [4–6, 10, 12–19], and several theories were proposed to explain the causes of this effect. The review of these theories is presented, for example, in [18]; here we give general ideas of these theories. In earlier papers [4–6, 12] constriction was considered as a consequence of non-uniform gas heating across the discharge and was attributed to the dependence of the local ionization–recombination balance of charged species on the gas temperature. Later on, so-called diffusion–recombination

theories [10, 13–17] were developed; the term 'diffusion' is used to emphasize the role of diffusion processes in charged species balance. In these theories, a strong non-linear dependence of the ionization rate on the electron concentration due to stepwise ionization processes and the influence of electron–electron (e–e) collisions on the shape of the electron energy distribution function (EEDF) and, respectively, on the excitation and ionization rate constants is considered as a key reason for constriction. Ambipolar diffusion is a major factor that withstands discharge constriction.

It was shown in [10, 15–17] that without taking into account e–e collisions constriction occurs gradually with the discharge current increase, and exact inclusion of e–e collisions into calculations of the EEDF leads to stepwise contraction in inert gases (except helium). Actually, the correct modelling of the constriction effect requires that both gas heating and non-linearity of the ionization/excitation rates as functions of the electron number density be taken into account. The general discussion of the constriction effects can be found, for example, in [1].

It was shown experimentally for argon and neon gases [8–10] that the stepwise contraction taking place at the current increase is followed by a similar stepwise transition to the diffuse form, if the discharge current then decreases. If the critical discharge current for the contraction is higher than that for reverse transition, the hysteresis effect takes place. Semi-analytic models developed in [10, 15, 17] were able to qualitatively explain the appearance of the hysteresis effects in Ne and Ar. A more accurate approach was realized in the paper [18] where the constriction effect in pure argon was studied numerically using a 1D axial-symmetric model. In this paper balance equations for the charged particles and for the populations of the excited states were solved in parallel with the equation for the gas temperature and the Boltzmann equation for the EEDF. A detailed kinetic model for the atomic and ionic species was used in calculations. Simulations were performed for the experimental conditions of [9]. The calculated $E(I)$ characteristics appeared to be in reasonable agreement with those measured in experiments, and results of simulations confirmed the conclusion made in [10, 15–17] about the dominant role of e–e collisions in the mechanism of constriction. However, the hysteresis effect was not reproduced in calculations. Recently, a numerical approach was employed for modelling of the constriction effect in neon [19] under experimental conditions [8], and hysteresis effect was observed in calculations. In [19] a simplified kinetic model for the excited neon atoms was used. The authors [19] claimed that their theory was unable to reproduce the hysteresis effect when using the local approximation for the EEDF. They suggested the approximation of the EEDF by a two-temperature Maxwellian distribution, and an effective temperature of its high-energy tail was found from an approximate non-local equation derived by the authors.

In the case of stepwise constriction the diverse time evolution of the positive column was observed. If the discharge current is rapidly increased from $I_1 < I_c$ to $I_2 \gg I_c$, then a virtually uniform constriction of the positive column along its full length occurs. In the case $I_2 \geqslant I_c$, when the discharge current slightly exceeds the critical value, the contraction occurs near one of the electrodes and evolves to the other electrode, i.e. the boundary between the constricted and diffuse parts of the positive column moves along the discharge tube. In some cases, the boundary can stop at some intermediate location between electrodes. If this is the case, then the so-called partially constricted glow discharge is realized. Such a kind of discharge was observed in 1966 in argon [20], but no special studies of it were carried out. In [21] it was briefly reported about the observation of the partially constricted glow discharge in an argon–nitrogen mixture. Recently, the existence of this effect in an argon–nitrogen mixture was confirmed in [22, 23]. As for pure argon, the possibility of such a kind of discharge is not quite clear now.

In this work the experimental and theoretical study of the constriction effect in the positive column of the glow discharge in argon is done. In order to study the hysteresis effect, voltage–current characteristics (VCCs) of the discharge were measured by two ways: increasing the current and decreasing the current. Special measures were undertaken to realize the partially contracted discharge.

A 1D axial-symmetric self-consistent discharge model was developed and implemented for numerical simulations of Ar discharge under experimental conditions. The description of the model is given and results of calculations, in particular, $E(I)$ characteristics, are presented in the paper. The calculated $E(I)$ characteristics are compared with those derived from experiment. For the first time, the detailed kinetic model without the usage of fit parameters predicts the hysteresis effect in pure Ar. The parameters of diffuse and constricted forms of the discharge are in good agreement with the experiment.

2. Experimental setup and procedures

The experimental setup is basically similar to that described in [21–23]. The cylindrical discharge tube, 3 cm i.d., was made of molybdenum glass. This tube from the anode end was connected to a narrow (2 cm i.d.) and short (2 cm length) tube. Then this construction was connected to glass tubes of 4.5 cm i.d. and of 3 cm length, which in turn were joined with extensions, where two identical cylindrical tantalum electrodes were placed. The distance between the electrodes was 75 cm. The narrow short tube initiates the discharge constriction from one end which allowed us to study the partial constriction. Gaseous argon (99.998% purity) was pumped through the set of liquid-nitrogen cooled traps and then through the discharge tube at a flow rate of ∼100 sccm (residence time in the discharge ∼1 min). Such a rate was low enough to avoid formation of a pressure gradient along the discharge. A 10 kV dc power supply could maintain the discharge current up to 100 mA. The discharge current could be changed by varying the power supply voltage V_s or changing the ballast resistance R_b. The latter was varied in the ∼0.1–1 MΩ range for obtaining ∼1–100 mA current values. For a given R_b value the discharge voltage drop and current were measured and recorded with a two-channel oscilloscope. This procedure took about 2–3 min and allowed one to collect ∼10^4 records within some range of the VCCs with a 10 ms sample time.

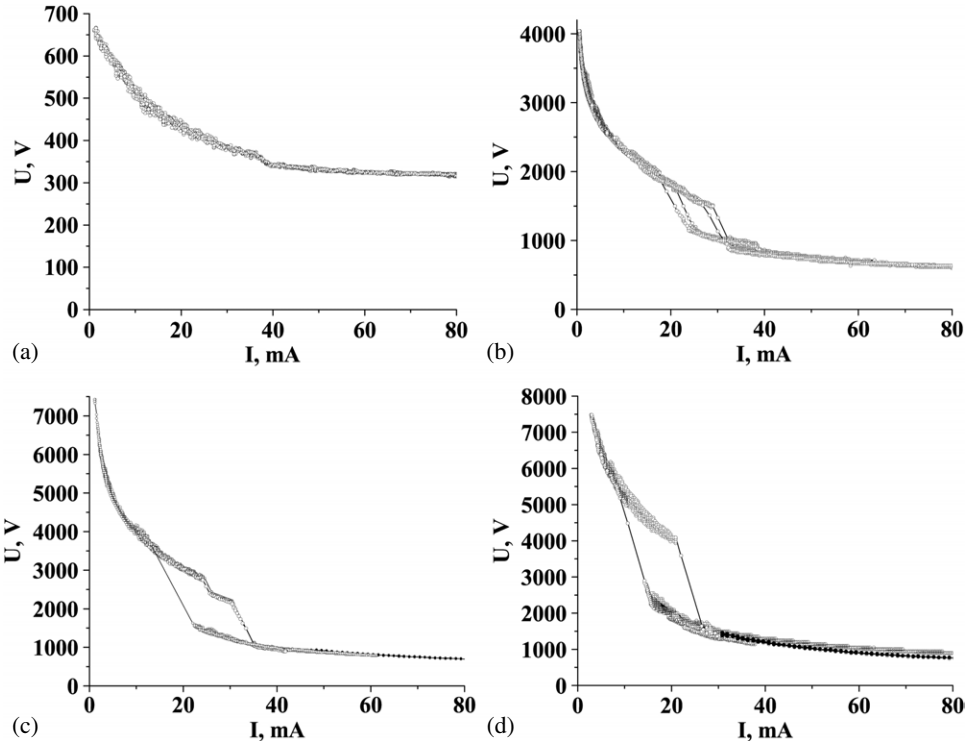

Figure 1. Voltage–current characteristics of the discharge measured at different argon pressures: $P = 5$ Torr (a), 40 Torr (b), 80 Torr (c) and 120 Torr (d).

About 5–10 different R_b values were used to extend the VCC ranges measured and to cover continuously the whole range of currents. Luminosity of the discharge was also studied with the use of an optical fibre that could be moved along the tube. A high speed CMOS camera pco.1200hs was used for taking the pictures of the discharge positive column.

In this study the gas pressure was varied from 1 to 120 Torr. Constriction of the discharge accompanied by jumps in the VCC was observed at $P > 20$ Torr. The results obtained for some of these conditions are shown in figures 1(a)–(d). Left and right branches of the VCCs in figures 1(b)–(d) correspond to diffuse and constricted forms of the discharge. Contraction is accompanied by a 1.5–2-fold lowering of the voltage at a small change in the current value. Transition between these two states occurs along the line

$$U + I R_b = V_s,$$

where U is the discharge voltage. In some cases the transition process extends in time up to about 0.1 s. Then the measurements allow us to resolve a few points along the transition line. Figure 1(c) exhibits an additional knee on the curve. In this case the discharge might contract at certain conditions in two steps. At first, the contraction starts from the anode to the narrow tube and then propagates at a larger current occupying the whole tube (see figure 1(c)). All the VCCs presented in figures 1(b)–(d) reveal a distinct hysteresis effect, namely, an essential difference between the curves obtained at current varying in the opposite directions.

At pressures lower than $P \approx 20$ Torr no jumps in VCCs were observed. Nevertheless, a bend in VACs was observed

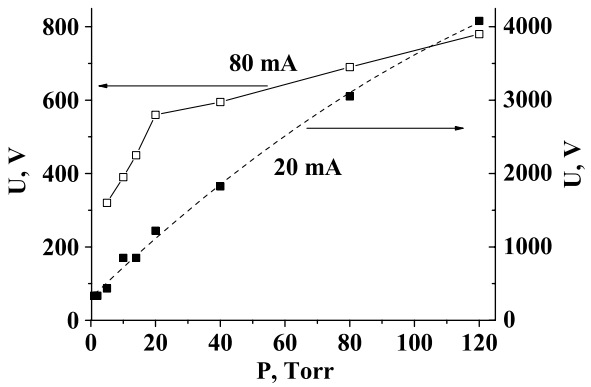

Figure 2. Discharge voltage drop as a function of gas pressure for diffuse ($I = 20$ mA) and contracted ($I = 80$ mA) discharges.

down to as low as $P = 5$ Torr (see figure 1(a)). At low pressures a gradual narrowing of the luminous column with increasing current took place. Figure 2 shows the discharge voltage as a function of pressure for two current values. Monotonic, near linear growth of U versus P is seen for the diffuse form of the discharge at current $I = 20$ mA. For $I = 80$ mA there is a sharp kink on the $U(P)$ curve at $P = 20$ Torr, that is, at the point where the discharge constricts. For the contracted discharge ($P > 20$ Torr) the $U(P)$ dependence is notably weaker.

No striations were observed in the diffuse form of the discharge, i.e. the positive column was uniform along the tube axis (see figure 3). Constriction of the discharge is accompanied by the appearance of moving striations, which lead to modulation of plasma luminosity. Figure 3 illustrates

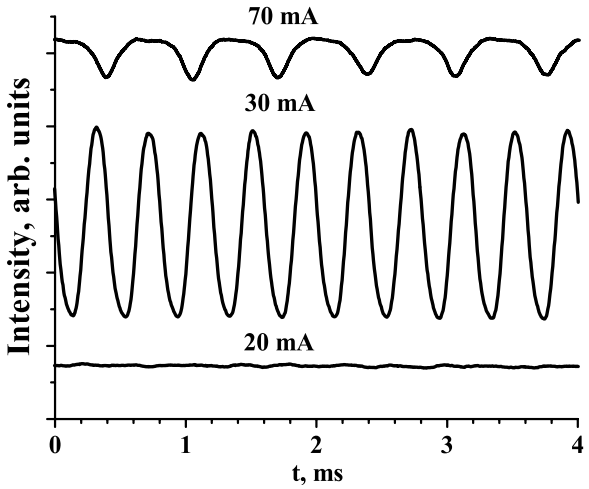

Figure 3. Time dependence of plasma local emission for diffuse ($I = 20$ mA) and contracted ($I = 30$ and $I = 70$ mA) discharges. $P = 40$ Torr.

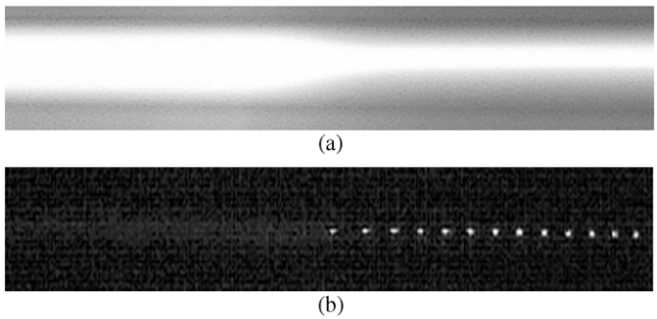

Figure 4. Picture of partially contracted discharge in argon (*a*) taken with long time exposition and (*b*) taken with 50 μs exposition (emission of the diffuse (left) part of the discharge is too weak for detection); the bright points in the contracted (right) part are the moving striations.

that the shape of modulation changed and its amplitude diminished with current. Pulsation frequency diminished with current and the pulsation shape changed from sinusoidal to markedly non-harmonic.

As a rule, the process of discharge constricting took less than ~0.1 s. However, in a few runs it was possible to observe an intermediate state of discharge with stable diffuse and contracted parts (see figure 4(*a*)), i.e. partial contraction took place, which was found previously in argon [20] and Ar–N_2 [21–23] discharges. In the contracted part of the discharge moving striations could be detected (see figure 4(*b*)). Let us note that in Ar : N_2 mixtures [21–23] a partially contracted discharge was easily reproduced and repeated, while in the case of argon it was observed rather accidentally than regularly.

3. Discharge model

To calculate the plasma parameters it was assumed that the discharge column is cylindrically symmetric and uniform along the tube axis. In this case, a 1D axial-symmetric discharge model for pure argon could be applicable. Our model includes balance equations for the charged species, a system of kinetic equations for populations of electronic states, an equation for the gas temperature and an equation for the electric circuit. The populations of two lower resonance states were calculated by taking into account resonance radiation transfer effects. Rate coefficients for electron-induced processes and electron transport coefficients were calculated by solving the electron Boltzmann equation in parallel with the system of kinetic equations. The atom density as a function of gas pressure and temperature was found from the ideal gas equation of state.

The electron Boltzmann equation was solved using the so-called two-term approximation for the electron velocity distribution function. For pure argon under glow discharge conditions this approximation is rather accurate to calculate the EEDF and relevant kinetic coefficients. It was also assumed that at every location the EEDF depends only on the local plasma parameters. For gas pressures and the tube radius under consideration such an assumption is evidently satisfied in the case of the diffuse form of discharge, when plasma fills the whole cross section of the tube. The problem of applicability of the local approach in the case of the contracted discharge where the transverse size of the plasma cord is small will be discussed in some detail in section 5. The Boltzmann equation for the EEDF was solved by the iteration method [24]. The following processes were taken into account (see table 1): elastic scattering of electrons from argon atoms, excitation of electronic states by electron impact from the ground state and stepwise excitation, ionization of atoms from the ground state and stepwise ionization, ionization of dimers, recombination of electrons with ions, dissociation of molecular ions by electron impact, appearance of electrons in Penning processes, e–e collisions and second kind collisions with excited atoms.

In the model two sorts of positive ions, Ar^+ and Ar_2^+, are taken into account and quasineutrality of plasma is assumed, that is, $n_e = [Ar^+] + [Ar_2^+]$ (concentrations of particular species are denoted by square brackets). In fact, Ar_3^+ ions are also formed in plasma, but according to calculations [18] the concentration of these ions is small with respect to the Ar_2^+ concentration, and they have no influence on the discharge behaviour.

The radial fluxes of electrons and ions were described in terms of ambipolar diffusion. For example, the balance equation for the electrons has the form

$$\frac{\partial n_e}{\partial t} - \frac{1}{r}\frac{\partial}{\partial r}\left(r D_a \frac{\partial n_e}{\partial r}\right) = \Gamma_{ion} - \Gamma_{rec}, \qquad (1)$$

where D_a is the ambipolar diffusion coefficient and Γ_{ion} and Γ_{rec} are the total ionization and recombination rates. In the case of two sorts of positive ions the ambipolar diffusion coefficient can be derived as

$$D_a \approx \frac{D_e}{\mu_e}\left(\frac{[Ar^+]}{n_e}\mu_1 + \frac{[Ar_2^+]}{n_e}\mu_2\right), \qquad (2)$$

where D_e is the free transverse diffusion coefficient of electrons, μ_e is the electron mobility and μ_1 and μ_2 are mobilities of atomic and molecular argon ions, respectively. The ions' mobility under normal conditions ($T_g = 300$ K and $P = 760$ Torr) was taken as $\mu_1 = 1.6\,\mathrm{cm^2\,V^{-1}\,s^{-1}}$ and

Table 1. Processes incorporated in the model.

Nos	Process	k ($cm^6\ s^{-1}$, $cm^3\ s^{-1}$, s^{-1})	References
	Elastic electron scattering		
1	$Ar + e \rightarrow Ar + e$	BE[a]	[32]
	Excitation from the ground state		
2	$Ar + e \leftrightarrow Ar(i) + e$, $i = 1s_5, 1s_4, 1s_3, 1s_2$	BE	[33]
3	$Ar + e \leftrightarrow Ar(F) + e$	BE	[33]
4	$Ar + e \leftrightarrow Ar(A) + e$	BE	[33]
5	$Ar + e \leftrightarrow Ar(B) + e$	BE	[33]
	Ionization from the ground state		
6	$Ar + e \rightarrow Ar(+) + e + e$	BE	[34]
	Mixing by electrons		
7	$Ar(i) + e \leftrightarrow Ar(j) + e$, $i, j = 1s_5, 1s_4, 1s_3, 1s_2$	$f(T_e)$	[35]
	Mixing by atoms		
8	$Ar(1s_5) + Ar \leftrightarrow Ar(1s_4) + Ar$	$2.3 \times 10^{-15}\ cm^3\ s^{-1}$	[36]
9	$Ar(1s_3) + Ar \leftrightarrow Ar(1s_4) + Ar$	$4.3 \times 10^{-15}\ cm^3\ s^{-1}$	[36]
	Stepwise excitation		
10	$Ar(i) + e \leftrightarrow Ar(F) + e$, $i = 1s_5, 1s_3$,	BE	See the text
11	$Ar(i) + e \leftrightarrow Ar(F) + e$, $i = 1s_4, 1s_2$	BE	See the text
12	$Ar(F) + e \leftrightarrow Ar(A) + e$	BE	See the text
13	$Ar(F) + e \leftrightarrow Ar(B) + e$	BE	See the text
14	$Ar(A) + e \leftrightarrow Ar(B) + e$	BE	See the text
	Stepwise ionization		
15	$Ar(i) + e \leftrightarrow Ar^+ + e + e$, $i = 1s_5, 1s_4, 1s_3, 1s_2$	BE	[42]
16	$Ar(F) + e \rightarrow Ar^+ + e + e$	BE	See the text
17	$Ar(A) + e \rightarrow Ar^+ + e + e$	BE	See the text
18	$Ar(B) + e \rightarrow Ar^+ + e + e$	BE	See the text
	Chemi-ionization		
19	$Ar(i) + Ar(j) \rightarrow Ar^+ + Ar + e$, $i, j = 1s_5, 1s_4, 1s_3, 1s_2$	$1.2 \times 10^{-9}\ cm^3\ s^{-1}$	[44,45], see the text
	Ion conversion		
20	$Ar + Ar^+ + Ar \rightarrow Ar_2^+ + Ar$	$2.3 \times 10^{-31}\ (300/T_g)^{0.67}\ cm^6\ s^{-1}$	[49]
	Dissociative recombination		
21	$Ar_2^+ + e \rightarrow Ar(A) + Ar$	BE	See the text
	Dissociation of molecular ions		
22	$Ar_2^+ + e \rightarrow Ar^+ + Ar + e$	BE	[54]
	Three-body recombination		
23	$Ar^+ + e + Ar \rightarrow Ar + Ar$	$2.3 \times 10^{-22}/T_g^{2.5}\ cm^6\ s^{-1}$	[55]
24	$Ar^+ + e + e \rightarrow Ar + e$	$2.1 \times 10^{-27}/T_e^{4.5}\ cm^6\ s^{-1}$	[55]
	Dimer formation		
25	$Ar^* + Ar + Ar \rightarrow Ar_2^* + Ar$	$1.4 \times 10^{-32}(300/T_g)^{0.5}\ cm^6\ s^{-1}$	[36], see the text
	Dimer ionization		
26	$Ar_2^* + e \rightarrow Ar_2^+ + e + e$	BE	[48], see the text
	Dimer emission		
27	$Ar_2^* \rightarrow Ar_2 + h\nu$	$10^6\ s^{-1}$	[48], see the text
	Emission		
28	$Ar(1s_4, 1s_2) \rightarrow Ar + h\nu$		See the text
29	$Ar(F) \rightarrow Ar(1s_5, 1s_4, 1s_3, 1s_2) + h\nu$	$1.6 \times 10^7, 9.3 \times 10^6, 3.0 \times 10^6, 8.5 \times 10^6\ s^{-1}$	See the text
30	$Ar(A) \rightarrow Ar(F) + h\nu$	$1.56 \times 10^7\ s^{-1}$	See the text
31	$Ar(B) \rightarrow Ar(A) + h\nu$	$8.6 \times 10^6\ s^{-1}$	See the text
32	$Ar(B) \rightarrow Ar(F) + h\nu$	$9.1 \times 10^5\ s^{-1}$	See the text
33	$Ar(B) \rightarrow Ar(1s_5, 1s_4, 1s_3, 1s_2) + h\nu$	$1.8 \times 10^5, 1.2 \times 10^5, 3.7 \times 10^4, 9.3 \times 10^4\ s^{-1}$	See the text

[a] means that rate constant is calculated from Boltzmann equation solution.

$\mu_2 = 2.7\ cm^2\ V^{-1}\ s^{-1}$ [25]. The dependence of ions' mobility on the gas temperature (for a fixed gas number density) was taken into account, and the necessary data were taken from [26].

The standard boundary conditions for equation (1) are

$$\frac{\partial n_e(0)}{\partial r} = 0, \qquad n_e(R) = 0, \tag{3}$$

where R is the tube radius. The same boundary conditions were used for ions.

The radial profile of the gas temperature was calculated by solving the thermal balance equation

$$\rho c_p \frac{\partial T_g}{\partial t} - \frac{1}{r}\frac{\partial}{\partial r}\left(r\lambda(T_g)\frac{\partial T_g}{\partial r}\right) = Q(r) \qquad (4)$$

with the boundary conditions

$$\frac{\partial T_g(0)}{\partial r} = 0, \qquad T_g(R) = T_w. \qquad (5)$$

In equations (4) and (5) ρ is the gas mass density, c_p is the thermal capacity, λ (T_g) is the thermal conductivity, $Q(r)$ accounts for the sources of gas heating and T_w is the gas temperature at the wall. In our calculations T_w is set at the 300 K value. Data for λ (T_g) were taken from [25]. In the temperature range 300–900 K, $\lambda(T_g)$ can be approximated with good accuracy by a linear function λ $(T_g) = 7.6063 \times 10^{-5} + 3.776 \times 10^{-7} T_g$ (W cm^{-1} K^{-1}). The heat source $Q(r)$ was calculated accurately in the kinetic block of our model. It is taken into account that the power density deposited in the discharge $Ej(r)$ ($j(r)$ is the current density) is dissipated not only to gas heating but also to processes of ionization, excitation of radiative states and some others.

In the balance equations for the populations of the electronic states diffusion of excited atoms to the tube wall, as well as different collisional and radiative processes, is taken into account (see the description of the kinetic model in the next section). The diffusion coefficient for excited atoms was taken as 0.09 cm^2 s^{-1} (under normal conditions) in accordance with [27].

For the two lower resonant states of argon ($1s_4$ and $1s_2$ states in the Paschen notation) radiation transfer effects were described in terms of the Holstein–Biberman equation [28]. In this case, the rate of population variation $Q_{res}(r)$ due to spontaneous emission and resonant radiation transport is written as [28]

$$Q_{res}(r) = -\frac{Ar^*(r)}{\tau} + \int Ar^*(r')K(|r - r'|)\,dr', \qquad (6)$$

where τ is the lifetime of the resonant state and the kernel of the integral is the function of the absolute value of the coordinate difference $\rho = |\boldsymbol{r} - \boldsymbol{r}'|$:

$$K(\rho) = -\frac{1}{4\pi\rho^2\tau}\frac{\partial f(\rho)}{\partial \rho}. \qquad (7)$$

Under the considered conditions, collisions with atoms dominate in spectral line broadening, so the probability f (ρ) of a photon propagating a certain distance ρ without being absorbed or scattered is described by the asymptotic expression: $f(\rho) = 1/\sqrt{\pi k_0 \rho}$. The absorption coefficient at the line centre k_0 is defined as $k_0 = 8\pi/\lambda$, where λ is the resonant transition wavelength. Data on τ and λ values were taken from [29]. The correct description of resonance radiation transfer is important in our problem, because it is one more factor acting against constriction.

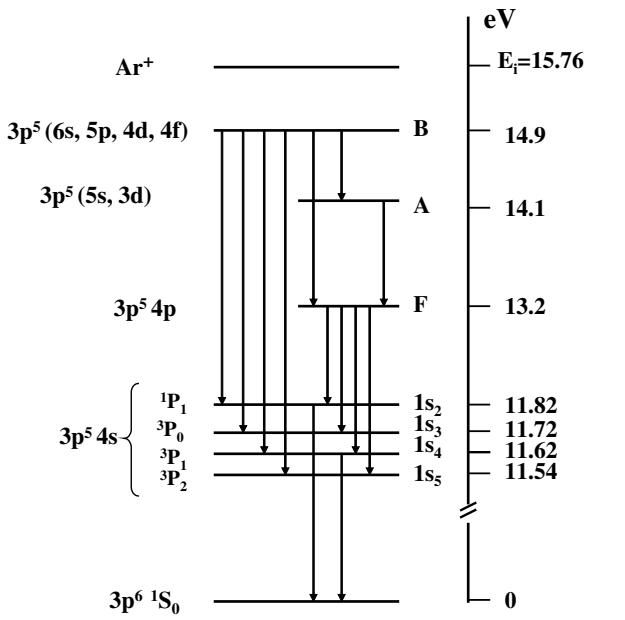

Figure 5. Schematic diagram of the electronic states of Ar involved in the kinetic model. Arrows represent considered optical transitions.

An exact solution of the balance equations comprising integral term (6) was found numerically using an algorithm developed in [30, 31].

The equation for the electric circuit was taken in the form

$$V_s = EL + IR_b,\ I = 2\pi\int_0^R rj(r)\,dr$$

$$= 2\pi eE\int_0^R rn_e(r)\mu_e(r)\,dr,$$

where V_s is the voltage applied across the positive column and the ballast resistor connected in series, E is the electric field strength in the positive column, L is the positive column length, $j(r)$ is the current density and e is the electron unit charge.

For a given tube length, tube radius, ballast resistor and argon pressure the input parameter of the model is the power supply voltage V_s. Starting from the initial radial profiles of concentrations of all the species and gas temperature evolution of the plasma parameters was calculated till convergence to steady state. For each value of V_s the electric field strength E in the positive column, discharge current I, the gas temperature distribution $T_g(r)$ and radial profiles of electrons, ions and excited atoms are calculated in a self-consistent manner. Finally, results of calculations can be represented as a function of the discharge current value.

4. Kinetic model

A schematic of the electronic states of Ar taken into account in the kinetic model is shown in figure 5, and the processes included in the model are listed in table 1. Let us consider the model in more detail. A rather complete kinetics of four lower electronic states of Ar is considered. Two of these levels ($1s_3$ and $1s_5$) are metastable, whereas the other two ($1s_4$ and $1s_2$) are resonance. The higher electronic states are combined into three

lumped levels (F, A and B) according to the recommendations of [28], with level F (13.2 eV) being the sum of the $3p^5 4p$ levels, level A (14.1 eV) being the sum of the $3p^5 5s$ and $3p^5 3d$ levels and the level B (14.9 eV) being the sum of the $3p^5 6s$, $3p^5 5p$, $3p^5 4d$ and $3p^5 4f$ levels. The populations of individual sublevels of lumped levels were assumed to be proportional to their statistical weights.

The momentum transfer cross section for the electron scattering from argon atoms (no 1 in table 1) was taken from [32]. Cross sections for the excitation of electronic levels from the ground state (nos 2–5 in table 1) were chosen according to recommendations of [33]. To derive cross sections for the excitation of lumped levels, the cross sections for corresponding individual sublevels were summed up. The cross section for ionization from the ground state (no 6 in table 1) was used the same as in [34].

Rate constants for the mixing of $3p^5 4s$ levels by electrons (no 7 in table 1) were taken from [35], where they are presented as a function of electron temperature. Mixing of metastable and resonance states by atoms (nos 8–9 in table 1) is also taken into account, corresponding rate constants were taken from [36].

Cross sections for electron impact excitation from $1s_5$ and $1s_3$ metastable levels to $3p^5 4p$ levels have been measured and computed [37–39]. In [35] a critical review of data published in [37–39] was made and a set of cross sections was constructed. In our model a similar approach for cross sections' construction was employed. Individual cross sections were then summed up to obtain cross sections for the excitation of the lumped F level (no 10 in table 1).

Cross sections for the stepwise excitation from $1s_4$ and $1s_2$ levels to $3p^5 4p$ states were estimated using the similarity function method proposed in [40] for optically allowed transitions. Most of the $1s_4 \rightarrow 3p^5 4p$ and $1s_2 \rightarrow 3p^5 4p$ transitions are optically allowed, so the corresponding cross sections were calculated using the formula derived in [40]. Data on optical transition probabilities needed for calculations were taken from [41]. Since the contribution of the optically forbidden transitions to summed cross sections for F level excitation (no 11 in table 1) is small, it was neglected.

A similar approach was used to calculate cross sections for the other stepwise processes (nos 12–14 in table 1); data on optical transition probabilities were taken from [41]. For each of these processes the lower electronic level is lumped one. In this case the total cross section was calculated as the sum of the cross sections for the transitions between individual sublevels weighted with statistical weights of lower sublevels.

Cross sections for the stepwise ionization from $3p^5 4s$ and $3p^5 4p$ levels (nos 15–16 in table 1) were taken from [42], and from A and B lumped levels (nos 17–18 in table 1) were estimated using the formula presented in [43].

The rate constant for chemi-ionization with the participation of Ar atoms in the $1s_5$ metastable state (no 19 in table 1) was taken from [44, 45]. The rate constants for similar reactions with the participation of Ar atoms in other $3p^5 4s$ states were assumed to be the same. In the review paper of Kolokolov and Blagoev [45] a tenable conclusion is made that (according to theoretical as well as experimental studies) for rare gases the output of molecular ions in metastable + metastable reactions is low. In particular, for argon the measured output of Ar_2^+ ions is about 5% with respect to the total ion output [46]. For this reason, production of molecular ions in metastable + metastable reactions was not taken into account in our model. It should be noted that in some papers it is assumed that the outputs of molecular and atomic ions are of the same order of magnitude [47] or the output of atomic ions is negligible [48]. The examination of references given in [47,48] showed that these assumptions are not supported by convincing arguments.

The rate constant for the three-body conversion of Ar^+ ions into Ar_2^+ ions (no 20 in table 1) was taken from [49], the temperature-dependent factor of this rate constant is $T_g^{-0.67}$. The cross section for the dissociative recombination of electrons with Ar_2^+ ions (no 21 in table 1) was assumed to be Cu^{-1}, where u is the electron energy. For such an energy dependence of the cross section and a Maxwellian EEDF, the recombination rate constant depends on the electron temperature T_e as $T_e^{-0.5}$, which agrees with theoretical and experimental data [50]. The normalizing factor C was fit to provide a rate constant value of 7×10^{-7} cm^3 s^{-1} at $T_e = 300$ K [50]. It is noted in [50] (with reference to [51]) that there are some evidences of the dependence of the recombination rate constant on the vibrational temperature of ions T_v, the vibration temperature factor is $\sim T_v^{-1}$. This effect is taken into account in our model assuming that the vibrational temperature is equal to the gas temperature. The reason for this assumption is that rate constants of V–T relaxation processes of molecular ions with argon atoms are high [52] because of high polarizability of argon atoms and a small value of the ion vibrational quantum ($\sim$0.015 eV) [53]. The process of dissociation of molecular ions by electron impact (no 22 in table 1) is also included in the model; the cross section for this process was taken from the theoretical work of [54].

Rate constants for the three-body recombination processes (nos 23–24 in table 1) were estimated using formulae presented in [55]. The kinetics of dimers is represented in the kinetic model by three reactions (nos 25–27 in table 1). The rate constant for the formation of dimers at $T_g = 300$ K was taken the same as in [36], and the temperature-dependent factor $T_g^{-0.5}$ was chosen in analogy with that for xenon dimers [56]. The cross section for the ionization of argon dimers by electron impact was also taken similar to that for xenon [56]. The effective lifetime of argon dimers was estimated to be 10^{-6} s [48].

As discussed above, for emission processes from $1s_2$ and $1s_4$ states (no 28 in table 1) resonant radiation transfer effects were taken into account. For radiative transitions between excited states, effects of radiation imprisonment can be neglected, since the populations of lower states for these optical transitions are low. Transition probabilities presented in table 1 for emission transitions from lumped levels (nos 29–33 in table 1) are effective probabilities. They were calculated as the sum of transition probabilities for the transitions between individual sublevels weighted with statistical weights of upper sublevels. Relevant data on optical transition probabilities were taken from [41].

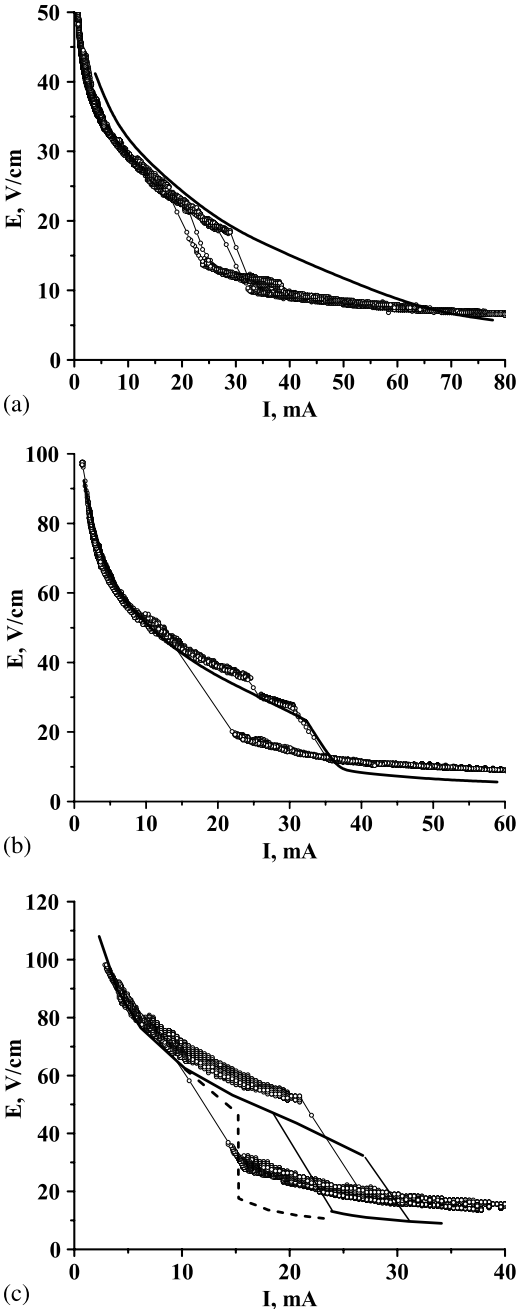

Figure 6. The comparison between experimental (narrow solid lines with symbols) and calculated (thick solid lines) values of the electric field strength in the positive column of the glow discharge in argon for $P = 40$ Torr (a), 80 Torr (b) and 120 Torr (c). The dashed line represents the result of calculations performed for $P = 120$ Torr without taking into account the gas temperature dependence of the dissociative recombination rate constant.

5. Results of modelling and discussion

Numerical simulations were performed for the discharge tube radius $R = 1.5$ cm and argon pressures $P = 40$, 80 and 120 Torr. Let us first present the results of calculations of the electric field strength in the positive column as a function of the discharge current value. Calculated $E(I)$ dependences are shown in figures 6(a)–(c) in comparison with those derived from the measured VCCs. Experimental values of the electric field strength were estimated as $E = (U - U_c)/L$, where U_c is the cathode voltage drop and L is the distance between electrodes. In the normal glow discharge the cathode voltage drop is almost independent of the discharge current and gas pressure and depends only on the cathode material and gas mixture [1]. In particular, for the glow discharge in pure argon the typical cathode voltage drop is about $U_c \approx 100$–130 V depending on the cathode material [1]. Since we did not find U_c data for tantalum electrodes used in our experiments, we assumed that $U_c = 120$ V and is independent of discharge conditions. In spite of some uncertainty in the choice of the U_c value, the presented formula gives good estimation of the electric field strength, since in experiments a rather long discharge tube was used so that the voltage drop across the positive column ($U - U_c$) was essentially higher than the cathode voltage drop (U_c) (compare the measured U values presented in figures 1(b)–(d) with $U_c = 120$ V).

The examination of figures 6(a)–(c) shows that for all considered gas pressures the calculated $E(I)$ characteristics are in good agreement with experimental data at low discharge currents, where the discharge exists in a diffuse form ($I <$ 30 mA for $P = 40$ and 80 Torr, $I < 22$ mA for $P = 120$ Torr). As for the modelling of the transition from the diffuse to the contracted form, the situation is different for different pressures.

In the case of $P = 40$ Torr (see figure 6(a)) the theoretical $E(I)$ characteristic displays a monotonic decrease in the whole range of currents, i.e. constriction occurs gradually with current. This is in contradiction to the experiment, where a stepwise decrease in $E(I)$ (i.e. the constriction of the positive column) is observed at $I = 30$ mA.

For the gas pressure $P = 80$ Torr (see figure 6(b)) our model reproduces an abrupt decrease in the electric field in the positive column observed in experiments at $I = 30$ mA, though the calculated electric field in the contracted discharge ($I > 37$ mA) is slightly lower than the experimental value. The difference between theory and experiment in this case is that the hysteresis effect is not found in calculations.

It was found that the hysteresis effect is reproduced in simulations for a higher argon pressure. It follows from our calculations (see figure 6(c)) that for $P = 120$ Torr the transition from the diffuse to the contracted form occurs at $I = 27$ mA and the reverse transition takes place at $I = 24$ mA. Respectively, in the range of discharge currents 24–27 mA the positive column can exist in the diffuse as well as in the contracted form. Though this current interval is narrower than the experimental one (16–22 mA) and is shifted towards higher currents, the most uncommon is the fact that the hysteresis is reproduced in a realistic kinetic model with an acceptable accuracy.

To get a better insight into the nature of constriction, information on plasma parameters is presented below. Gas temperature, mean electron energy, electron concentration and ions' densities at the axis of the discharge tube calculated for different argon pressures are shown in figures 7(a)–(d) as a function of the discharge current value. It follows from figure 7(a) that noticeable deviations in the temperature from 300 K (the temperature at the tube wall) appear at rather

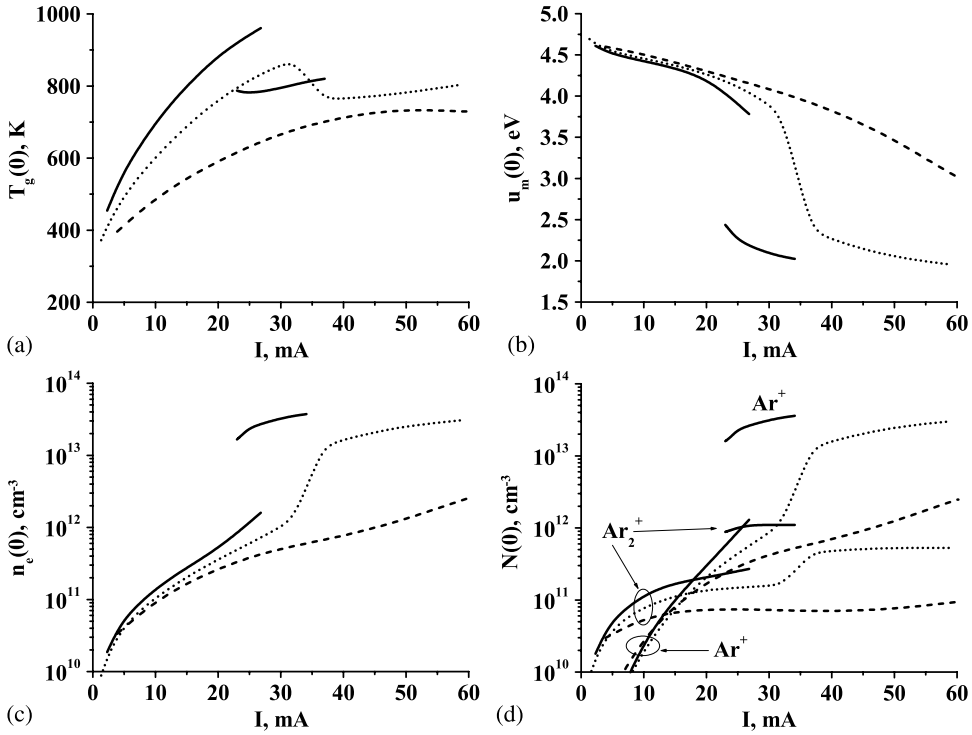

Figure 7. Gas temperature (*a*), mean electron energy (*b*), electron concentration (*c*) and ions densities (*d*) at the axis of the discharge tube calculated for $P = 40$ Torr (----), 80 Torr (· · · · · ·) and 120 Torr (——) as a function of the discharge current value.

low currents (∼2 mA). For gas pressure $P = 40$ Torr the gas temperature at the tube axis (see figure 7(*a*)) increases monotonically with current up to the value of about 740 K. For gas pressures $P = 80$ Torr and 120 Torr the gas temperature sharply increases with current (up to 870 K and 960 K, respectively) while the discharge exists in the diffuse form. The contraction of the positive column leads to the decrease in the gas temperature; this is due to a considerable decrease in the discharge power with respect to that of the diffuse discharge. In the constricted discharge the gas temperature at the tube axis also increases with current but not so fast as in the diffuse discharge.

The mean electron energy at the tube axis (see figure 7(*b*)) in plasma of the diffuse discharge slightly decreases with current (from $u_m \sim 4.5$ eV at $I = 5$ mA to $u_m \sim 4$ eV at $I = 25$ mA) and for a given current value it is almost independent of the gas pressure. In plasma of the contracted discharge the mean electron energy is about two times lower (∼2 eV) and also decreases with current. This is explained by the low value of the electric field strength in the contracted positive column (see figure 6). Let us note that the EEDF in the argon plasma under the considered conditions is not a Maxwellian one in the whole range of electron energies, especially in the case of the low ionization degree. For this reason, the u_m value characterizes the main body of the EEDF but not its high-energy tail, which governs the excitation rates of electronic levels from the ground state by electron impact.

At the transition to the contracted form of the discharge electron and ion concentrations at the tube axis (see figure 7(*c*)–(*d*)) exhibit an abrupt increase of more than one order of magnitude and attain values about 3.5×10^{13} cm^{-3} ($P = 120$ Torr). At low discharge currents ($I < 15$ mA) Ar_2^+ is the dominant ion in plasma, while at higher currents Ar^+ ion dominates.

The ratio of Ar^+ and Ar_2^+ concentrations in the diffuse discharge depends on the rate of Ar^+ production, Q_i. Since the decay of atomic ions is governed by the process of ion conversion (no 20 in table 1), their concentration is proportional to Q_i, $[Ar^+] \sim Q_i$. Molecular ions are produced in the reaction of ion conversion, so their production rate is also close to Q_i. Ar_2^+ ions decay in processes of dissociative recombination with electrons and dissociation by electron impact (nos 21–22 in table 1). Setting $n_e = [Ar_2^+]$ (this is not valid at high currents, but is reasonable for the estimations) one can obtain that $[Ar_2^+] \sim Q_i^{1/2}$. Since $[Ar^+] \sim Q_i$ and $[Ar_2^+] \sim Q_i^{1/2}$, at low discharge currents (low Q_i values) Ar_2^+ is the dominant ion in plasma, while at high discharge currents (high Q_i values) Ar^+ ions dominate. The value of the discharge current, at which the concentrations of atomic and molecular ions equalize, depends on the gas pressure.

Populations of some excited states at the tube axis calculated for $P = 120$ Torr are shown in figure 8(*a*) as a function of the discharge current. The most populated level is the lower metastable one; in the contracted discharge its population is about 10^{12} cm^{-3}. Populations of higher electronic states (F and B in figure 8(*a*)) in the diffuse discharge are relatively small and increase considerably at the transition to the contracted form of discharge.

The lower (4s) states of argon atom are excited by electron impact from the ground state; the rate of populating (and population itself) is proportional to the electron concentration. The higher electronic level (F) is populated due to stepwise excitation processes. The rate of populating is proportional to

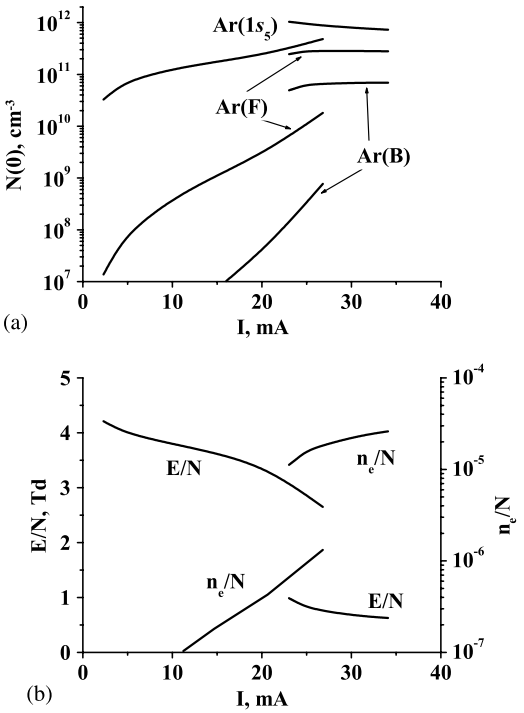

Figure 8. Populations of some excited states (*a*) and reduced electric field and ionization degree (*b*) at the axis of the discharge tube calculated for argon pressure $P = 120$ Torr as a function of the discharge current value.

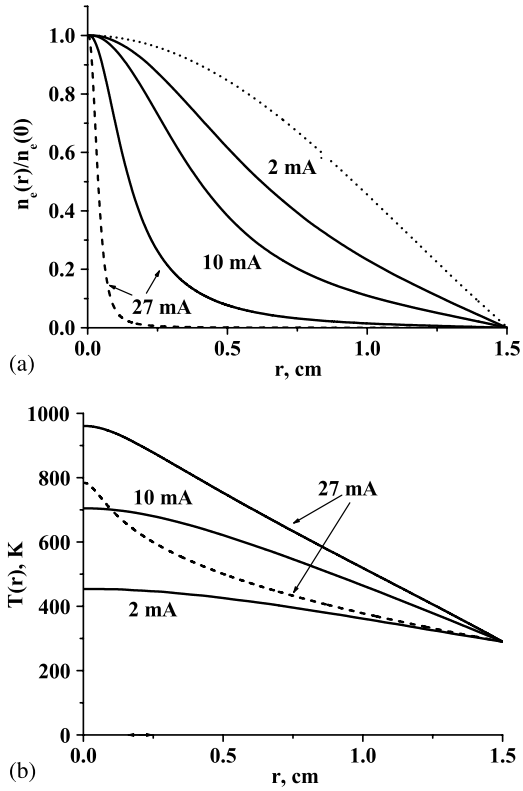

Figure 9. Radial profiles of the normalized electron concentration (*a*) and gas temperature (*b*) calculated for argon pressure $P = 120$ Torr and different discharge currents. Solid lines depict results for the diffuse discharge and dashed lines represent results for the contracted discharge. The Bessel profile is shown by the dotted line.

the population of lower states and the electron concentration, so the population of the F state is $\sim n_e^2$. In general, the higher the level, the stronger the dependence of its population on the electron concentration. In the diffuse discharge the concentration of electrons is relatively low and the populations of higher electronic states are small with respect to that of the lower metastable state. The increase in the electron concentration at the transition to the contracted form of discharge leads to considerable growth in higher levels' population.

Figure 8(*b*) illustrates the variation of the reduced electric field and ionization degree at the tube axis with discharge current for the gas pressure $P = 120$ Torr. The E/N parameter falls down with current in both diffuse and constricted forms. The ionization degree in plasma of the contracted discharge becomes as high as 3×10^{-5}.

In figure 9(*a*) the calculated radial profiles of the normalized electron concentration are shown for the gas pressure $P = 120$ Torr and different discharge currents. For the sake of comparison the classical Bessel profile (the profile of the fundamental diffusion mode in cylindrical geometry) is also shown in figure 9(*a*). It follows from figure 9(*a*) that even for a low discharge current ($I = 2$ mA) the calculated profile differs from the Bessel one. The higher the discharge current, the narrower the radial profile of the electron concentration. In the hysteresis region, there is an essential difference between the profile widths in diffuse and contracted discharges operated at the same discharge current (27 mA). The degree of the profile constriction can be characterized by the ratio of the electron concentration at the tube axis to the mean electron concentration (averaged over the cross section of the discharge tube) $\gamma = n_e(0)/\overline{n_e(r)}$; for the Bessel profile $\gamma \sim 2.3$. In calculations we have $\gamma = 3.9, 6.7$ and 32 for $I = 2$ mA, 10 mA and 27 mA (for diffuse discharge) and $\gamma = 720$ for $I = 27$ mA (contracted discharge). The effective radius of the contracted positive column estimated at a level of e^{-1} of the normalized electron concentration profile is about $r_c = 0.05$ cm.

Figure 9(*b*) depicts the radial distributions of the gas temperature calculated for the same value of gas pressure and discharge currents as in figure 9(*a*). The remarkable feature in figure 9(*b*) is that the shapes of the gas temperature distributions for different currents in the diffuse discharge are rather smooth, while in the case of the contracted discharge there is pronounced peaking of the temperature profile at the tube axis. Such variations in the gas temperature profiles are in agreement with experimental data measured for diffuse [57,58] and contracted [58] discharges.

Figure 10 shows the radial distributions of electron and ion concentrations in the contracted discharge ($P = 120$ Torr, $I = 27$ mA). We can see that within the effective radius of the positive column the concentration of molecular ions is almost independent of position and is small with respect to that of atomic ions. The concentration of Ar^+ diminishes rapidly while moving off the axis, so at the distance $\sim 2r_c$ from the tube axis concentrations of Ar^+ and Ar_2^+ become equal. Outside the cylinder with radius $2r_c$ molecular ions dominate.

Under the considered conditions the main source of molecular ions is the process of ion conversion

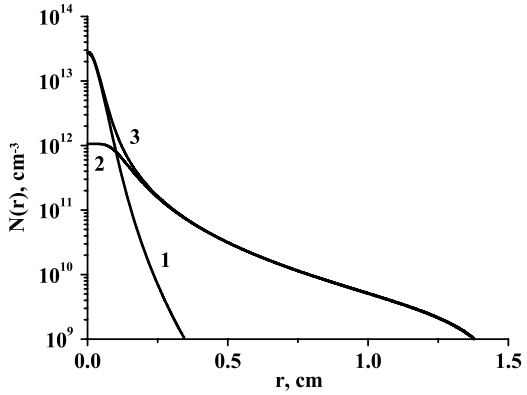

Figure 10. Radial profiles of Ar^+ (1), Ar_2^+ (2) and n_e (3) concentrations in the contracted positive column calculated for argon pressure $P = 120$ Torr and the discharge current value $I = 27$ mA.

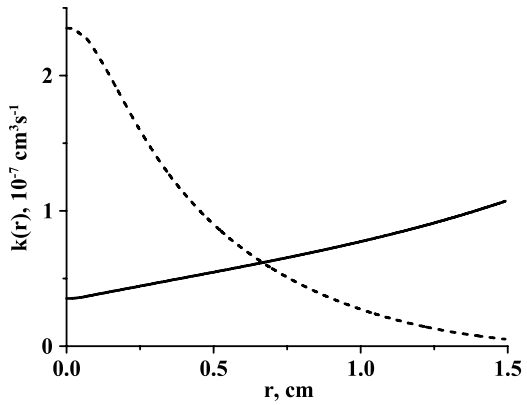

Figure 11. The rate constant for the dissociation of molecular ions by electron impact (----) and dissociative recombination rate constant (——) calculated as a function of the radial coordinate. Contracted discharge, $P = 120$ Torr, $I = 27$ mA.

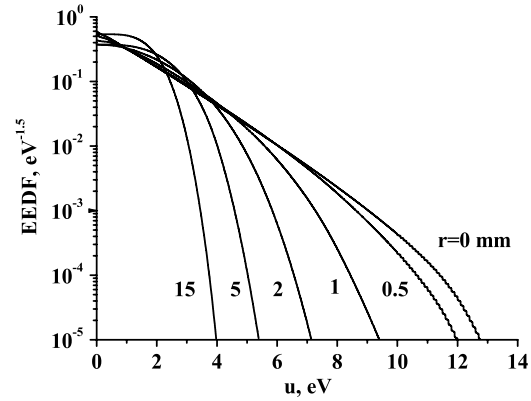

Figure 12. The EEDFs in the contracted positive column calculated at different locations along the tube radius. $P = 120$ Torr, $I = 27$ mA.

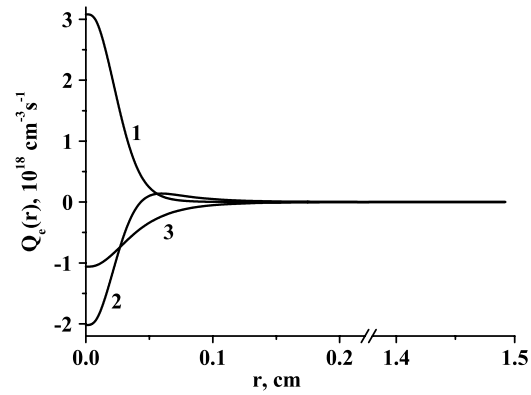

Figure 13. The radial distributions of ionization (1), ambipolar diffusion (2) and recombination (3) rates in the contracted discharge calculated for $P = 120$ and $I = 27$ mA.

(no 20 in table 1), and two competitive processes control the losses of Ar_2^+: dissociation by electron impact (no 22 in table 1) and the dissociative recombination with electrons (no 21 in table 1). Our calculations predict that at the tube axis the rate of Ar_2^+ ions decay due to their dissociation by electron impact is higher than that due to dissociative recombination with electrons. To illustrate this fact, in figure 11 the rate constants of both processes are shown as a function of the radial coordinate. It follows from figure 11 that at the axis dissociation rate constant $k_d(0)$ is about 6 times higher than the recombination rate constant $k_r(0)$. The variation of these rate constants with distance from the axis is entirely different: the value of k_d sharply diminishes, while the k_r value increases, dissociative recombination prevails over dissociation only at $r > 0.7$ cm. Such behaviour of rate constants is explained by the form of respective cross sections and by the variation of the EEDF along the tube radius. EEDFs in contracted discharge calculated at different radial positions from $r = 0$ to $r = 1.5$ cm are shown in figure 12. The reduced electric field changes from $E/N = 0.75$ Td at the tube axis to $E/N = 0.27$ Td at the tube wall due to the profile of the gas number density. The ionization degree in the considered case varies from 1.9×10^{-5} ($r = 0$) to zero ($r = 1.5$ cm). It follows from figure 12 that the population of the high-energy tail of the EEDF remarkably diminishes with distance; this is not only due to the decrease in the E/N value but also because of the lowering of the role of e–e collisions in EEDF formation. The mean electron energy calculated from the EEDF decreases from 2.2 eV ($r = 0$) to 1.3 eV ($r = 1.5$ cm).

The threshold energy for the process of Ar_2^+ dissociation by electron impact is about 2.7 eV and the cross section has a maximum at 4 eV [54]. For this reason, lowering of the tail of the EEDF leads to the decrease in the dissociation rate constant. The dissociative recombination rate constant $k_r \sim T_e^{-0.5}$ slightly increases with the variation of the mean electron energy from 2.2 to 1.3 eV. The noticeable rise in k_r along the tube radius shown in figure 11 is due to the gas temperature-dependent factor (see section 4).

In figure 13 the radial profiles of ionization, recombination and ambipolar diffusion rates in the contracted discharge ($P = 120$ Torr, $I = 27$ mA) are shown. Under the considered conditions, stepwise ionization is the dominant ionization process. Due to the narrow radial distributions of electrons and excited atoms as well as due to the radial variation of the EEDF (discussed above) the ionization rate sharply decreases with the radial coordinate. The decrease in the recombination rate with distance from the axis is essentially slower. Close to the axis the ionization rate is higher than the rate of recombination and the balance of electrons is provided by

ambipolar diffusion losses. At a distance of about 0.04 cm from the axis the diffusion rate changes the sign and diffusion plays the role of the electron source (i.e. the balance of inward and outward diffusion fluxes of electrons is positive). At larger off-axis distances (>0.055 cm) the ambipolar diffusion rate is higher than the ionization rate and is balanced by the recombination rate. The described behaviour of different terms in the electron balance equation is in agreement with results of other theoretical papers [14, 15, 18].

It is known that for the appearance of the constriction effect the non-linear (super-linear) dependence of the ionization frequency on the electron concentration is needed [1]. A few mechanisms are taken into account in the model which provide such dependence and provoke the constriction of the glow discharge: the increase in the excitation and ionization rate constant due to the influence of the e–e collisions on the shape of the EEDF, stepwise ionization processes and non-uniform gas heating, which leads to the increase in the E/N parameter in the centre of the tube. The most important mechanism which prevents the positive column from constriction is the ambipolar diffusion of electrons from the tube axis towards the tube wall. The higher the gas pressure, the lower the role of ambipolar diffusion and the more favourable are the conditions for the jump-like discharge constriction and hysteresis effect. This tendency is observed in experiments (compare VCCs showed in figures 1(*a*)–(*c*) as well as in calculations (see figures 6(*a*)–(*c*)). The quantitative difference between experiment and theory is that in calculations the hysteresis effect is predicted at gas pressures $P = 120$ Torr, while in experiments it is observed at $P = 40$ Torr. There are a few possible reasons for this discrepancy.

First of all, at current values where transition from the diffuse to the contracted discharge occurs the theoretical $E(I)$ characteristic is rather sensitive to the exact rate constant values for various processes, in particular to their dependences on gas temperature. To illustrate this fact, we have made calculations (for $P = 120$ Torr), in which the dissociative recombination rate constant was used without taking into account the gas temperature-dependent factor (coming from vibrational kinetics of ions). The calculated $E(I)$ characteristic is shown in figure 6(*c*) by the dashed line. One can see that in this case the transition from the diffuse to the contracted form of discharge takes place at lower discharge currents and no hysteresis effect is observed. Unfortunately, the gas temperature (vibrational temperature of ions) dependence of rate constants for some important processes is unknown. Such a situation is, for example, for dissociation of molecular ions by electron impact.

As follows from our calculations for $P = 120$ Torr, the effective radius of the contracted positive column is about 0.05 cm and is of the same order of magnitude as the characteristic length of the EEDF relaxation. It means that the non-local effects of the EEDF formation should be taken into account in the model, while in our calculations the EEDF was considered as a local function of plasma parameters.

The ionization degree at the tube axis in the contracted discharge is higher than 10^{-5} (see figure 8(*b*)), so the contribution of electron–ion Coulomb collisions to the total electron momentum transfer cross section can be noticeable at low electron energies [59]; this effect was not taken into account in our model.

Finally, let us note that there is a fundamental difference between experimental observations and assumptions made in our model. In the model the diffuse discharge, as well as the contracted discharge, is treated as the axially uniform one, while in experiments moving striations are always observed in the contracted positive column (see figures 3 and 4).

6. Conclusions

The transition from the diffuse to the contracted form of the glow discharge in argon was studied both experimentally and theoretically. Experiments were carried out in a wide range of argon pressures (1–120 Torr) and discharge currents (1–100 mA). VCCs as well as luminosity of discharge were measured. It was found that for a given discharge tube (3 cm i.d.) at pressures $P > 20$ Torr stepwise discharge constriction takes place at some critical current value; the constriction is accompanied by a 1.5–2-fold drop of the discharge voltage. For these pressures the measured $U(I)$ characteristics exhibit the classical hysteresis effect, i.e. the transition from the diffuse to the contracted discharge occurs at a current higher than that for reverse transition. At pressures $P < 20$ Torr a gradual narrowing of the luminous column with current growth occurs. No jumps in VCCs were observed in this case, though an insignificant bend does exist even at $P = 5$ Torr. It was demonstrated that constriction of the discharge is accompanied by initiation of moving striations; the amplitude and frequency of striations decrease with current. It was also found that in some cases the stable partially contracted form of discharge is realized, when the diffuse and contracted forms simultaneously exist in the discharge tube. It appeared that in argon this form of discharge is poorly reproducible.

The 1D axial-symmetric discharge model for pure argon was developed to investigate the discharge properties under experimental conditions. This model is based on solutions of balance equations for the charged particles, a system of kinetic equations for populations of electronic states, the equation for the gas temperature and the equation for the electric circuit, coupled with the Boltzmann equation for the EEDF. The resonance radiation transfer effects (for two lower resonant states of argon atom) are taken into account in terms of the Holstein–Biberman equation.

Simulations were performed for argon pressures of $P = 40$, 80 and 120 Torr. For these pressures the radial distributions of various plasma parameters were calculated for different discharge currents. The calculated $E(I)$ characteristics were compared with the experimental ones. Good agreement with experimental data was observed at low discharge currents where the discharge exists in a diffuse form. $E(I)$ calculated for the constricted form is in reasonable agreement with the experiment (within the 30% range). For the gas pressure of $P = 120$ Torr our model reproduced stepwise $E(I)$ variation as well as hysteresis effect. In the case of pressure $P = 80$ Torr the calculated $E(I)$ characteristic reveals stepwise behaviour similar to that observed in experiments, but

the hysteresis effect is not predicted in computations. For $P = 40$ Torr the model predicts the monotonic decrease of the $E(I)$ characteristic in the whole range of currents. Finally, probable causes for the difference between theoretical and experimental results are discussed.

Acknowledgment

This work was supported by the Russian Foundation for Basic Research # 06-02-17272.

References

[1] Raizer Yu P 1987/1991 *Gas Discharge Physics* (Moscow: Nauka,1987; Berlin: Springer-Verlag, 1991)
[2] Golubovskii Y B 2000 *Encyclopedia of Low-Temperature Plasma* ed V E Fortov (Moscow: Nauka) Introductory Volume, book II, p 40 (in Russian)
[3] Golubovskii Y B, Kudryavtsev A A, Nekuchaev V O, Porokhova I A and Tsendin L D 2004 *Electron Kinetics in Non-equilibrium Gas-discharge Plasma* (St Petersburg: St Petersburg University Publishing House) (in Russian)
[4] Kenty C 1962 *Phys. Rev.* **126** 1235
[5] Massey J T and Cannon S M 1965 *J. Appl. Phys.* **36** 361
[6] Massey J T 1965 *J. Appl. Phys.* **36** 373
[7] Baranov V Yu and Ul'yanov K N 1969 *Zh. Tekh. Fiz.* **39** 249
Baranov V Yu and Ul'yanov K N 1969 *Sov. Phys.—Tech. Phys.* **14** 176
[8] Golubovskii Yu B, Zinchenko A K and Kagan Yu M 1977 *Zh. Tekh. Fiz.* **47** 1478
Golubovskii Yu B, Zinchenko A K and Kagan Yu M 1977 *Sov. Phys.—Tech. Phys.* **22** 851
[9] Golubovskii Yu B and Sonneburg R 1979 *Zh. Tekh. Fiz.* **49** 295
Golubovskii Yu B and Sonneburg R 1979 *Sov. Phys.—Tech. Phys.* **24** 173
[10] Golubovskii Yu B and Sonneburg R 1979 *Zh. Tekh. Fiz.* **49** 754
Golubovskii Yu B and Sonneburg R 1979 *Sov. Phys.—Tech. Phys.* **24** 437
[11] Toader E I 1995 *J. Phys. D: Appl. Phys.* **28** 75
[12] Baranov V Yu and Ul'yanov K N 1969 *Zh. Tekh. Fiz.* **39** 259
Baranov V Yu and Ul'yanov K N 1969 *Sov. Phys. Tech.—Phys.* **14** 183
[13] Eletskii A V and Smirnov B M 1970 *Zh. Tekh. Fiz.* **40** 1682
Eletskii A V and Smirnov B M 1971 *Sov. Phys.—Tech. Phys.* **15** 1308
[14] Golubovskii Yu B and Lyagushchenko R 1977 *Zh. Tekh. Fiz.* **47** 1852
Golubovskii Yu B and Lyagushchenko R 1977 *Sov. Phys.—Tech. Phys.* **22** 1073
[15] Golubovskii Yu B and Sonneburg R 1979 *Zh. Tekh. Fiz.* **49** 302
Golubovskii Yu B and Sonneburg R 1979 *Sov. Phys.—Tech. Phys.* **24** 177
[16] Golubovskii Yu B, Nekuchaev V O and Pelyukova E B 1996 *Zh. Tekh. Fiz.* **66** 43
Golubovskii Yu B, Nekuchaev V O and Pelyukova E B 1996 *Tech. Phys.* **41** 254
[17] Golubovskii Yu B, Nekuchaev V O and Pelyukova E B 1966 *Zh. Tekh. Fiz.* **66** 76
Golubovskii Yu B, Nekuchaev V O and Pelyukova E B 1966 *Tech. Phys.* **41** 1011
[18] Petrov G M and Ferreira C M 1999 *Phys. Rev.* E **59** 3571
[19] Shkurenkov I A, Mankelevich Yu A and Rakhimova T V 2007 *Russian Conf. on Physics of Low Temperature Plasma (Petrozavodsk, Russia, 24–28 June 2006)* vol 1 p 155 (contributed papers)
[20] Garscadden A and Lee D A 1966 *Int. J. Electron.* **20** 567
[21] Ionikh Y Z, Chernysheva N V, Macheret S O and Miles R B 1999 *Bull. Am. Phys. Soc.* **44** 77
[22] Dyatko N A, Ionikh Y Z, Meshchanov A V, Napartovich A P and Yuretskiy A V 2006 *18th Europhysics Conf. on the Atomic and Molecular Physics of Ionized Gases (XVIIIth ESCAMPIG) (Lecce, Italy, 12–16 July 2006)* p 209 (Abstracts of Invited Lectures and Contributed Papers)
[23] Dyatko N A, Ionikh Y Z, Meshchanov A V and Napartovich A P 2006 *AIP Conf. Proc.* **876** 15
[24] Dyatko N A, Kochetov I V and Napartovich A P 1992 *Fiz. Plazmy* **18** 888
Dyatko N A, Kochetov I V and Napartovich A P 1992 *Sov. J. Plasma Phys.* **18** 462
[25] Kikoin I K (ed) 1976 *Tables of Physical Quantities* (Moscow: Atomizdat) (in Russian)
[26] Chanin L M and Biondi M A 1957 *Phys. Rev* **106** 473
[27] Tachibana K 1986 *Phys. Rev. A* **34** 1007
[28] Biberman L M, Vorob'ev V S and Yakubov I T 1982/1987 *Kinetics of Nonequilibrium Low-Temperature Plasmas* (Moscow: Nauka, 1982; New York: Consultants Bureau, 1987)
[29] Radtsig A A and Smirnov B M 1985/1986 *Reference Data on Atoms, Molecules and Ions* (Moscow: Energoatomizdat, 1986; Berlin: Springer, 1985)
[30] Lawler J E, Parker G J and Hitchon W N G 1993 *J. Quant. Spectrosc. Radiat. Transfer* **49** 627
[31] Parker G J, Hitchon W N G and Lawler J E 1993 *J. Phys. B: At. Mol. Opt. Phys.* **26** 4643
[32] Pack J L, Voshall R E, Phelps A V and Kline L E 1992 *J. Appl. Phys.* **71** 5363
[33] Yanguas-Gil A, Cotrino J and Alves L L 2005 *J. Phys. D: Appl. Phys.* **38** 1588
[34] Rapp D and Englander-Golden P 1965 *J. Chem. Phys.* **43** 1464
[35] Donnelly V M 2004 *J. Phys. D: Appl. Phys.* **37** R217
[36] Dyatko N A, Ionikh Yu Z, Meshchanov A V and Napartovich A P 2005 *Fiz. Plazmy* **31** 939
Dyatko N A, Ionikh Yu Z, Meshchanov A V and Napartovich A P 2005 *Plasma Phys. Rep.* **31** 871
[37] Boffard J B, Piech G A, Gehrke M F, Anderson L W and Lin C C 1999 *Phys. Rev.* A **59** 2749
[38] Bartschat K and Zeman V 1999 *Phys. Rev.* A **59** R2552
[39] Dasgupta A, Blaha M and Giuliani J L 1999 *Phys. Rev.* A **61** 012703
[40] Eletskii A V and Smirnov B M 1983 *Sov. Phys.—JETP* **84** 1639 (in Russian)
[41] Katsonis K and Drawin H W 1980 *J. Quant. Spectrosc. Radiat. Transfer* **23** 1
[42] Hyman H A 1979 *Phys. Rev.* A **20** 855
[43] Vainstein L A, Sobelman I I and Yukov E A 1979 *Excited Atoms and the Spectral Line Broadening* (Moscow: Nauka, 1979) p 128 (in Russian)
[44] Kolokolov N B 1985 *Plasma Chemistry* vol 13 ed B M Smirnov (Moscow: Energoatomizdat) (in Russian)
[45] Kolokolov N B and Blagoev A B 1993 *Usp. Fiz. Nauk* **163**(3) 55
Kolokolov N B and Blagoev A B 1993 *Phys. Usp.* **36**(3) 152
[46] Borisov V B, Egorov V S and Ashurbekov N A 1983 *IV All-Union Conf. on Physics of Low-Temperature Plasma (Leningrad, Russia, 1983)* p 20 (Abstracts of Papers) (in Russian)
[47] Bogaerts A and Gijbels R 1999 *J. Appl. Phys.* **86** 4124
[48] Neeser S, Kunz T and Langhoff H 1997 *J. Phys. D: Appl. Phys.* **30** 1489
[49] Lui W F and Conway D C 1975 *J. Chem. Phys.* **62** 3070
[50] Biondi M A 1976/1982 *Principles of Laser Plasmas* ed G Bekefi (New York: Wiley, 1976; Moscow: Energoatomizdat, 1982)
[51] Cunningham A J and Hobson R M 1969 *Phys. Rev.* **185** 98
[52] Ivanov V A 1992 *Usp. Fiz. Nauk.* **35**(1) 17

Ivanov V A 1992 *Sov. Phys.—Usp.* **35**(1) 17
[53] Onuma T, Yoshii H, Ishijima H, Itou Y, Hayaishi T and Morioka Y 1999 *J. Mol. Spectrosc.* **198** 209
[54] Marchenko V S 1983 *Sov. Phys.—JETP* **83** 500 (in Russian)
[55] Zhilinskii A G (ed) 1994 *Handbook on Rate Constants for Processes with Atoms, Ions, Electrons, Photons* (St Peterburg: St Peterburg University Publishing House) (in Russian)
[56] Eckstrom D J, Nakano H H, Lorents D C and Rothem T 1988 *J. Appl. Phys.* **64** 1679
[57] Yalin A P, Ionikh Y Z and Miles R B 2002 *Appl. Opt.* **41** 3753
[58] Yalin A P 2000 Gas Phase and Plasma Diagnostics Based on Resonant Atomic Vapor Filters *PhD Dissertation*, Princeton University
[59] Kortshagen U and Schluter H 1992 *J. Phys. D: Appl. Phys.* **25** 644